Mars Water-Ice Clouds and Precipitation

J. A. Whiteway, *et al.*

Science **325**, 68 (2009);
DOI: 10.1126/science.1172344

The following resources related to this article are available online at www.sciencemag.org (this information is current as of July 21, 2009):

Updated information and services, including high-resolution figures, can be found in the online version of this article at:
http://www.sciencemag.org/cgi/content/full/325/5936/68

Supporting Online Material can be found at:
http://www.sciencemag.org/cgi/content/full/325/5936/68/DC1

A list of selected additional articles on the Science Web sites **related to this article** can be found at:
http://www.sciencemag.org/cgi/content/full/325/5936/68#related-content

This article **cites 15 articles**, 1 of which can be accessed for free:
http://www.sciencemag.org/cgi/content/full/325/5936/68#otherarticles

This article has been **cited by** 1 articles hosted by HighWire Press; see:
http://www.sciencemag.org/cgi/content/full/325/5936/68#otherarticles

This article appears in the following **subject collections**:
Planetary Science
http://www.sciencemag.org/cgi/collection/planet_sci

Information about obtaining **reprints** of this article or about obtaining **permission to reproduce this article** in whole or in part can be found at:
http://www.sciencemag.org/about/permissions.dtl

Science (print ISSN 0036-8075; online ISSN 1095-9203) is published weekly, except the last week in December, by the American Association for the Advancement of Science, 1200 New York Avenue NW, Washington, DC 20005. Copyright 2009 by the American Association for the Advancement of Science; all rights reserved. The title *Science* is a registered trademark of AAAS.

Mars Water-Ice Clouds and Precipitation

J. A. Whiteway,[1]* L. Komguem,[1] C. Dickinson,[1] C. Cook,[1] M. Illnicki,[1] J. Seabrook,[1] V. Popovici,[1] T. J. Duck,[2] R. Davy,[1] P. A. Taylor,[1] J. Pathak,[1] D. Fisher,[3] A. I. Carswell,[4] M. Daly,[5] V. Hipkin,[6] A. P. Zent,[7] M. H. Hecht,[8] S. E. Wood,[9] L. K. Tamppari,[8] N. Renno,[10] J. E. Moores,[11] M. T. Lemmon,[12] F. Daerden,[13] P. H. Smith[11]

The light detection and ranging instrument on the Phoenix mission observed water-ice clouds in the atmosphere of Mars that were similar to cirrus clouds on Earth. Fall streaks in the cloud structure traced the precipitation of ice crystals toward the ground. Measurements of atmospheric dust indicated that the planetary boundary layer (PBL) on Mars was well mixed, up to heights of around 4 kilometers, by the summer daytime turbulence and convection. The water-ice clouds were detected at the top of the PBL and near the ground each night in late summer after the air temperature started decreasing. The interpretation is that water vapor mixed upward by daytime turbulence and convection forms ice crystal clouds at night that precipitate back toward the surface.

The seasonal hydrological cycle on Mars is most evident in the Arctic region, where the atmospheric water vapor abundance increases to a maximum in midsummer after the seasonal ground ice cover reaches a minimum (*1*). The water returns to the surface as the atmosphere cools in late summer, but it has not previously been known whether this process involves clouds and precipitation as on Earth. Observations of water vapor and temperature during the Viking missions indicated that the atmosphere would be saturated with respect to water ice at night (*2*, *3*), and it was suggested that the precipitation of ice crystals could be an important factor for the exchange of water between the atmosphere and surface (*4*). Here we report on experimental evidence that clouds and precipitation play a role in the exchange of water between the atmosphere and ground on Mars.

The Phoenix mission (*5*, *6*) obtained measurements from the surface in the Arctic region of Mars (68.22°N, 234.25°E). The spacecraft landed before the summer solstice on Mars and operated over the next 5 months. This period encompasses the midsummer peak and decline in the abundance of atmospheric water vapor, so it was possible to observe the local processes that contribute to the water cycle. The Phoenix mission included a light detection and ranging (LIDAR) instrument (*7*) that emitted pulses of laser light upward into the atmosphere and detected the backscatter from dust and clouds. An essential capability of the LIDAR was that it could resolve the internal structure of water-ice clouds that drifted past the landing site.

Daytime LIDAR observations mainly detected dust in the atmosphere. The measurements on the 45th sol (*8*) after landing were typical for moderate dust loading with no clouds (Fig. 1A). The dust was distributed evenly up to a height of 4 km because of the daytime vertical mixing produced by convection and turbulence within the planetary boundary layer (PBL). The atmospheric dust loading reached a peak around the summer solstice and then generally decreased. On sol 97 [solar longitude of Mars (L_s) = 121°], the dust loading within the PBL was reduced by a factor of 3 in comparison with that on sol 45 (Fig. 1A).

During the period around the summer solstice, clouds were observed sporadically and mainly above heights of 10 km. Moving into late summer, 50 sols after the solstice (L_s = 113°), the LIDAR detected a regular pattern of cloud formation each night within the PBL. A shallow surface-based cloud formed near midnight (Mars local solar time), and a second cloud layer formed after 1 a.m. at heights around 4 km. On sol 99 (L_s = 122°), there was a clear enhancement in the extinction coefficient due to the presence of clouds in the height range from 3 to 4 km and in the layer up to 1 km above the ground (Fig. 1B). The observed clouds formed at an estimated temperature of around –65°C (Fig. 1C), which is consistent with clouds that are composed of water-ice crystals (the frost point for carbon dioxide is less than –120°C). On each sol during the second half of the mission (L_s = 113° to 150°), clouds remained through the early morning hours and then dissipated when the atmosphere warmed sufficiently during the daytime. As the summer progressed toward autumn and the air temperature decreased, the clouds persisted longer into the morning hours and ex-

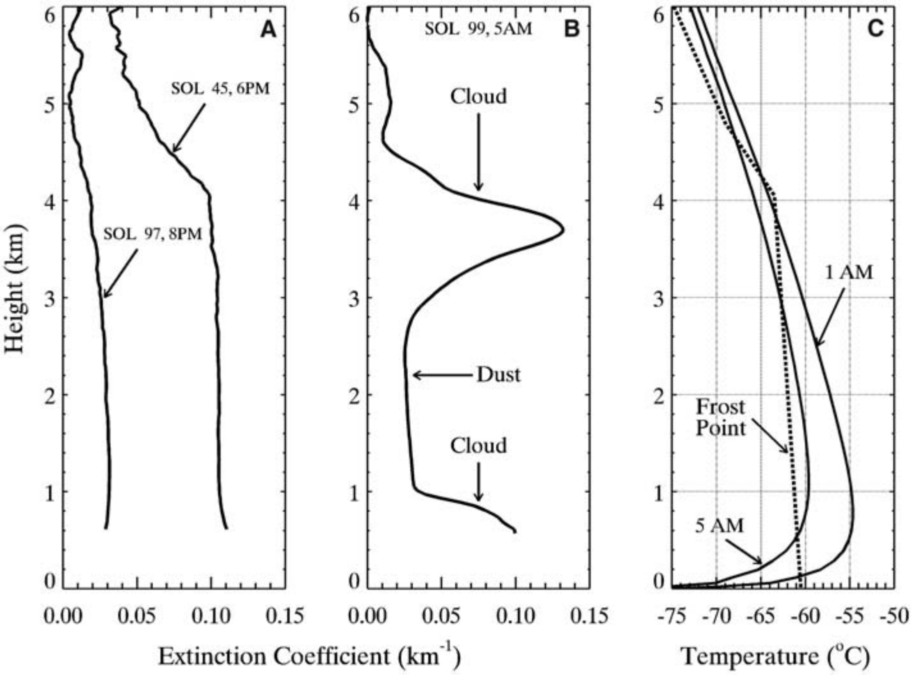

Fig. 1. (**A** and **B**) Profiles of the optical extinction coefficient (*9*) derived from the LIDAR backscatter signal at wavelength 532 nm for sols 45 (L_s = 97°), 97 (L_s = 121°), and 99 (L_s = 122°). Each profile is averaged over 1 hour and smoothed for a vertical resolution of 40 m. (**C**) Height profiles of atmospheric temperature estimated with a numerical simulation model of the martian PBL (*19*, *20*), and an estimate of the profile of frost point temperature.

---

[1] Department of Earth and Space Science and Engineering, York University, Toronto, Ontario, Canada. [2] Department of Physics and Atmospheric Science, Dalhousie University, Halifax, Nova Scotia. [3] National Glaciology Group, Geological Survey of Canada, Natural Resources Canada, Ottawa, Ontario, Canada. [4] Optech, Vaughan, Ontario, Canada. [5] MacDonald, Dettwiler and Associates (MDA), Brampton, Ontario, Canada. [6] Canadian Space Agency (CSA), St-Hubert, Quebec, Canada. [7] NASA Ames Research Center, Moffett Field, CA, USA. [8] Jet Propulsion Laboratory, California Institute of Technology, Pasadena, CA, USA. [9] Department of Earth and Space Sciences, University of Washington, Seattle, WA, USA. [10] Department of Atmospheric, Oceanic and Space Sciences, University of Michigan, Ann Arbor, MI, USA. [11] Department of Planetary Sciences, University of Arizona, Tucson, AZ, USA. [12] Department of Atmospheric Sciences, Texas A&M University, College Station, TX, USA. [13] Belgian Institute for Space Aeronomy (BIRA-IASB), Brussels, Belgium.

*To whom correspondence should be addressed. E-mail: whiteway@yorku.ca

tended further toward the ground. Clouds were not detected in the late afternoon or evening.

The outline and internal structure of the clouds that drifted above the Phoenix landing site are seen in the contour of the backscatter coefficient (*9*). On sol 99 (Fig. 2A), the most striking features are the tilted vertical streaks after 05:00 (Mars local time). This pattern is consistent with ice crystals precipitating from the cloud and eventually sublimating in the subsaturated air below the cloud. Such fall streaks are a well-known feature in observations of cirrus clouds on Earth.

In the early morning hours on sol 109, the LIDAR observed clouds and precipitation that extended all the way to the ground (Fig. 2B). In the period between 03:10 and 03:50, there were water-ice clouds at the top of the PBL (at heights of 3 to 5 km) and at ground level. In the next LIDAR run, from 05:16 to 05:45, the base of the observed cloud had dropped to a height of about 1.5 km, and there were precipitation fall streaks starting at 05:30 that extended down through the ground-level cloud. The LIDAR is not able to measure below about 50 m because of the geometry of the transmitter/receiver overlap. It is reasonable to assume that the ice crystals would have continued to descend through the saturated air to reach the surface. The essential point here is that precipitation moves water toward the surface from heights of up to 5 km (*10*).

In the period around sol 99 (L_s = 122°), clouds were observed only after 01:00, so we take this as the time when clouds were initially forming. The average fall speed required to produce a fall streak length of 1.2 km (Fig. 2A) after 4 hours is consistent with an ellipsoidal ice particle with an aspect ratio of 3 and volume equivalent to a sphere with a radius of 35 μm (*11*). This approximates a columnar ice crystal 42 μm wide and 127 μm long, which is similar to ice crystals that have been sampled in cirrus clouds on Earth (*12*, *13*). The comparison is not surprising, because cirrus clouds on Earth form at a similar temperature and water vapor density.

The extinction coefficient represents the effective cross-sectional area of the ice crystals per unit of volume and, assuming spherical particles, the ice water content can be calculated as IWC = $4\sigma R_{\mathrm{eff}}\rho/3Q$. σ is the extinction coefficient; R_{eff} is the effective radius, which we assumed to be 35 μm based on the calculation of fall speed; Q is the scattering efficiency, which has a value of 2; and ρ is the density of water ice. The enhancement in the extinction coefficient due to the cloud in the average signal profile (Fig. 1B) has a peak value of 0.1 km^{-1}, but the range is from 0.07 to 0.27 km^{-1} in profiles with shorter averages. The corresponding estimates of IWC for spherical particles are in the range of 1.5 to 5.8 mg m^{-3}, and this is also similar to measurements of cirrus clouds on Earth (*14*). The spherical assumption can be avoided by using the empirical relationship between the extinction coefficient and IWC that was derived from aircraft in situ measurements in cirrus clouds (*14*): IWC = 119 $\sigma^{1.22}$. This gives a similar range of values: 1.0 to 5.3 mg m^{-3}. Using the empirical relationship, the amount of ice water integrated in the vertical (from the mean profile of Fig. 1B) is 1.9 g m^{-2}, which has the same value in units of precipitable micrometers (pr-μm) of water. This is more than substantial enough to play a role in the seasonal decreasing trend of about 0.5 pr-μm per sol in the local column water vapor (from L_s = 120° to 160°) measured from orbit (*1*).

We estimated the amount of water vapor within the PBL from the height and time of cloud formation, combined with the simulated temperature. For cloud formation commencing at 01:00 at a height of 4 km, the simulated temperature is –64.3°C (Fig. 1C), and the corresponding saturated vapor pressure is 0.61 Pa. The threshold relative humidity over ice for nucleation on desert dust has been measured in the laboratory to be in the range from 110 to 130% (*15*). Thus, we assumed that the water vapor pressure at a height of 4 km when the cloud started to form was 20% greater than the saturated value: 0.61 × 1.2 = 0.73 Pa. At the height of 4 km, the water vapor volume mixing ratio before cloud formation is 0.73/522 = 0.0014, where the model atmospheric pressure is 522 Pa. The uncertainty in this estimate is about ±20%, based on the range in the possible cloud formation times and the ice nucleation threshold. It is also assumed here that water vapor was well mixed throughout the PBL by the daytime

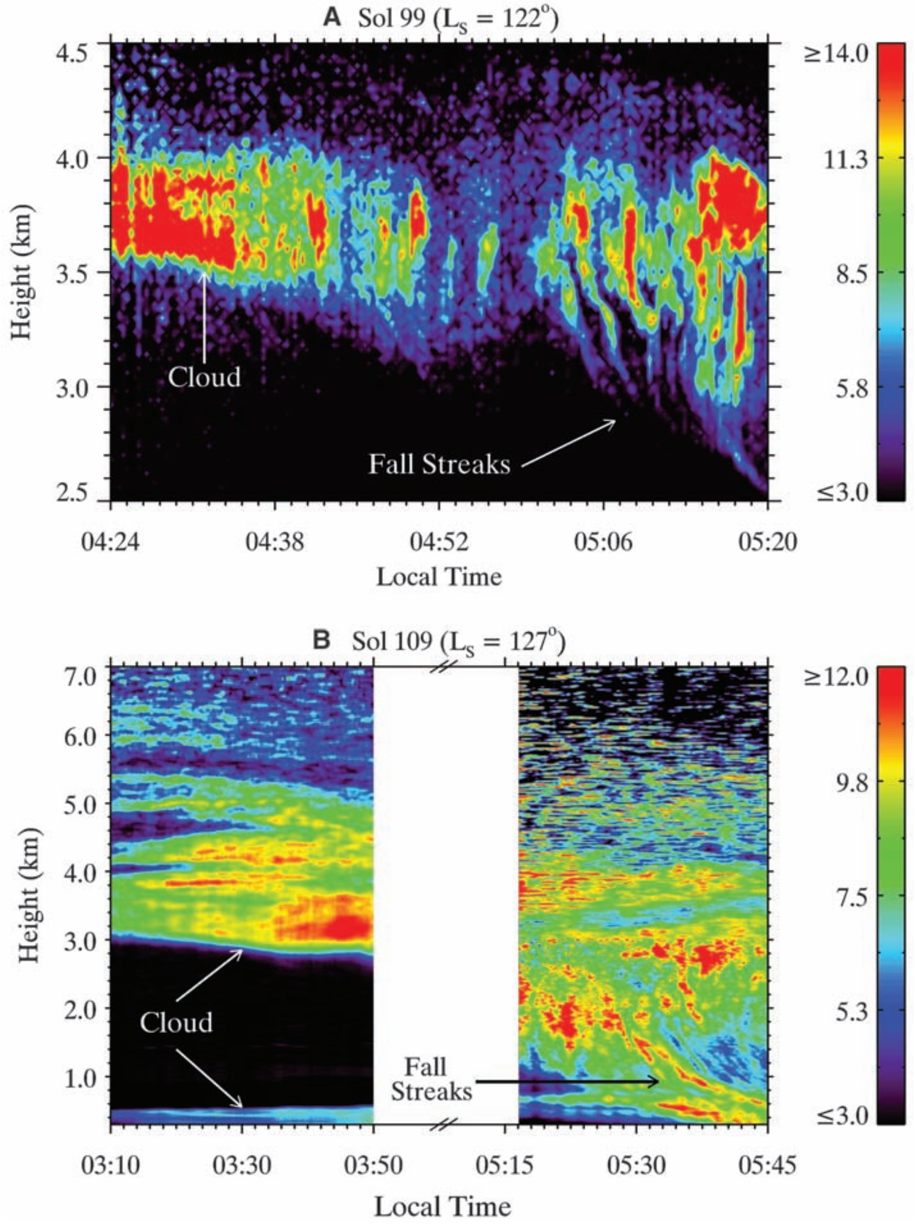

Fig. 2. Contour plots of backscatter coefficient ($\times 10^{-6}$ m^{-1} sr^{-1}) derived from the LIDAR backscatter signal (*9*) at wavelength 532 nm on mission sols 99 (L_s = 122°) (**A**) and 109 (L_s = 127°) (**B**).

turbulence and convection, so that in the early evening, the mixing ratio of water vapor was approximately constant up to a height of 4 km. Above the cloud top, the water vapor partial pressure would have been below the saturation value because clouds were not observed at those heights. The corresponding height profile of frost point temperature (before cloud formation) is shown in Fig. 1C. The integrated amount of water vapor within the PBL (from the ground to 4 km) before cloud formation on sol 99 (L_s = 122°) can be estimated from the analysis above to be 35 pr-µm. This is a substantial fraction of the total atmospheric column water vapor (40 to 50 pr-µm) measured from orbit at the latitude of Phoenix in previous years (*1*, *16*). Solar radiation measurements during the Pathfinder mission also indicated that atmospheric water vapor was confined near the ground (*17*).

We also used the simulated temperature profiles in Fig. 1C to estimate the IWC in the clouds. At 05:00 and a height of 4 km, the simulated temperature is –66°C and the saturated vapor density is 5 mg m^{-3}. The threshold value of vapor density at cloud formation (time 01:00) was 7.6 mg m^{-3}. The difference of 2.6 mg m^{-3} is an estimate of the IWC in the cloud, and this is within the range of IWC derived from the LIDAR measurements.

Our estimate of the water content of the PBL is consistent with independent measurements. The Thermal and Electrical Conductivity Probe instrument (*18*) on Phoenix measured the partial pressure of water vapor near the ground to have values up to 2 Pa during the daytime and less than 0.1 Pa at night, with a diurnal average of 0.9 Pa (*6*). The water vapor volume mixing ratio in the mixed boundary layer would be greater than the average at ground level (0.0012), because the vertical mixing occurs mainly during the daytime. Also, if the water vapor volume mixing ratio was 0.0016 throughout the PBL, then the integrated amount up to a height of 4 km would be 40 pr-µm, and this is an upper limit because it is within the measured range of the total atmospheric column water vapor (*1*, *16*). Our estimate of the volume mixing ratio at the top of the PBL (0.0014) is within the range of plausible values.

The Phoenix LIDAR observations have demonstrated that water-ice crystals grow large enough to precipitate through the atmosphere of Mars. In the early morning hours, the clouds formed at ground level and at heights around 4 km because these were the coldest parts of the PBL (Fig. 1C). The cloud was capped at the top of the PBL because daytime turbulent mixing does not transport moisture above that height. The overall process was that water ice was transported downward by precipitation at night, it sublimated in the morning, and then the vapor was mixed back up through the PBL by turbulence and convection during the daytime. The clouds and precipitation act to confine water within the PBL. Eventually the ice clouds would have persisted within the PBL throughout the daytime, and water ice would have remained deposited on the ground. As the depth of the PBL decreased in late summer, this local process would contribute to the seasonal decrease in atmospheric water vapor (*1*).

References and Notes

1. M. D. Smith *et al.*, *J. Geophys. Res.* **107**, 5115 10.1029/2001JE001522 (2002).
2. D. Davies, *J. Geophys. Res.* **84**, 8335 (1979).
3. J. Ryan *et al.*, *J. Geophys. Res.* **87**, 7279 (1982).
4. R. A. Kahn, *J. Geophys. Res.* **95**, 14677 (1990).
5. P. H. Smith *et al.*, *J. Geophys. Res.* **113**, E00A18 (2008).
6. P. H. Smith *et al.*, *Science* **325**, 58 (2009).
7. J. A. Whiteway *et al.*, *J. Geophys. Res.* **113**, E00A08 10.1029/2007JE003002 (2008).
8. A sol is a martian day, with a length of 24.6 hours. Phoenix landed 30 sols before the Mars summer solstice, when solar longitude is L_s = 90°.
9. Materials and methods are available as supporting material on *Science* Online.
10. Further evidence of precipitation was observed in images of low-level clouds (supporting online material text).
11. N. A. Fuchs, *The Mechanics of Aerosols* (Pergamon, New York, 1964).
12. J. A. Whiteway *et al.*, *Geophys. Res. Lett.* **31**, L24102 (2004).
13. M. W. Gallagher *et al.*, *Q. J. R. Meteorol. Soc.* **131**, 1143 (2005).
14. A. J. Heymsfield *et al.*, *Geophys. Res. Lett.* **32**, L10807 (2005).
15. P. R. Field *et al.*, *Atmos. Chem. Phys.* **6**, 2991 (2006).
16. H. Tschimmel *et al.*, *Icarus* **195**, 557 (2008).
17. D. V. Titov *et al.*, *J. Geophys. Res.* **104**, 9019 (1999).
18. A. P. Zent *et al.*, *J. Geophys. Res.* **114**, E00A27 (2009).
19. R. Davy *et al.*, *J. Geophys. Res.* **114**, D04108 (2009).
20. For the simulations used here, the upper-level wind was assumed to be as 5 m s^{-1}. The temperature and pressure at ground level were matched to the Phoenix in situ measurements, and the height distribution of dust was based on the Phoenix LIDAR observations. The model predicts a PBL depth of 4 km, which is consistent with the LIDAR daytime dust observations (Fig. 1A).

21. We acknowledge contributions to landed operations from the engineering staff at the CSA (P. Allard, C. Brunet, D. Cormier, I. Tremblay, and E. Vachon) and MDA Space Missions (D. Hill, L. Clark, A. Kerr, and R. McCoubrey). This work was enabled by funding from the CSA under contract 9F007-070437/001/SR. The Phoenix mission was led by the University of Arizona, on behalf of NASA, and managed by the Jet Propulsion Laboratory.

Supporting Online Material

www.sciencemag.org/cgi/content/full/325/5936/68/DC1
Materials and Methods
SOM Text
Fig. S1
Movie S1
References

16 February 2009; accepted 27 May 2009
10.1126/science.1172344

A Coherent Single-Hole Spin in a Semiconductor

Daniel Brunner,[1] Brian D. Gerardot,[1] Paul A. Dalgarno,[1] Gunter Wüst,[1] Khaled Karrai,[2] Nick G. Stoltz,[3] Pierre M. Petroff,[3] Richard J. Warburton[1,4]*

Semiconductors have uniquely attractive properties for electronics and photonics. However, it has been difficult to find a highly coherent quantum state in a semiconductor for applications in quantum sensing and quantum information processing. We report coherent population trapping, an optical quantum interference effect, on a single hole. The results demonstrate that a hole spin in a quantum dot is highly coherent.

Semiconductor heterostructures can be designed to confine electrons, holes, and photons in specific ways. Post-growth processing enables the creation of individual devices and their interconnection into fully functional circuits. However, it is not yet clear whether these material advantages can be exploited in a new class of device whose operation depends on the controlled manipulation of coherent quantum states. Achieving the necessary coherence poses considerable challenges.

In bulk semiconductors and quantum wells, individual quantum states lose coherence rapidly through an interaction with the lattice vibrations, or phonons. An electron spin interacts only indirectly via the spin-orbit interaction with the phonons and emerges as a strong candidate quantum bit (qubit) (*1*). However, to suppress the spin-orbit interaction, the electron must be tightly confined to a nanoscopic quantum dot (*2*–*4*). But in GaAs, the semiconductor with the best materials properties, the electron spin now interacts with 10^4 to 10^5 nuclear spins, too few for cancellation of the hyperfine interaction and too many for each nuclear spin to be used as a resource. The nuclear spins create a fluctuating effective magnetic field, the Overhauser field. The electron spin precesses in the Overhauser field such that the time-averaged coherence time, T_2*, is small, just ~10 ns (*5*–*7*), much less than the intrinsic decoherence time, T_2, which is around 1 µs (*8*, *9*). This difficulty represents a stumbling block in engineering a coherent semiconductor spin state.

---

[1]School of Engineering and Physical Sciences, Heriot-Watt University, Edinburgh EH14 4AS, UK. [2]Department für Physik der Ludwig-Maximilians-Universität, Geschwister-Scholl-Platz 1, 80539 Munich, Germany. [3]Materials Department, University of California, Santa Barbara, CA 93106, USA. [4]Department of Physics, University of Basel, Klingelbergstrasse 82, 4056 Basel, Switzerland.

*To whom correspondence should be addressed. E-mail: r.j.warburton@hw.ac.uk